



引文格式: 王必任, 滕超, 白相东, 等. 北山造山带尖山子新元古代早期似斑状花岗岩年代学、地球化学特征及地质意义[J]. 西北地质, 2024, 57(6): 44–57. DOI: 10.12401/j.nwg.2024074

Citation: WANG Biren, TENG Chao, BAI Xiangdong, et al. Age, Geochemistry and Geological Significance of an Early Neoproterozoic Porphyritic Granite in the Jianshanzi Area of the Beishan Orogenic Belt[J]. Northwestern Geology, 2024, 57(6): 44–57. DOI: 10.12401/j.nwg.2024074

北山造山带尖山子新元古代早期似斑状花岗岩年代学、 地球化学特征及地质意义

王必任^{1,2}, 滕超^{3,*}, 白相东¹, 关成尧¹, 袁四化¹, 张晓飞⁴, 杨欣杰³

(1. 防灾科技学院地球科学学院, 河北 三河 065201; 2. 河北省地震动力学重点实验室, 河北 三河 065201; 3. 中国地质调查局自然资源实物地质资料中心, 河北 三河 065201; 4. 中国地质调查局发展研究中心, 北京 100037)

摘要: 笔者报道了北山造山带东缘尖山子地区新元古代早期似斑状花岗岩年代学、地球化学特征, 结合已发表的同期花岗质岩石地球化学数据, 讨论其源区性质及北山南部前寒武纪基底与塔里木克拉通的亲缘性。似斑状花岗岩两件样品锆石 U-Pb 年龄分别为 (901 ± 5) Ma, (935 ± 3) Ma, 表明其形成于新元古代早期。似斑状花岗岩样品发育钾长石斑晶, 显示高的 SiO_2 含量 ($70.41\% \sim 76.05\%$) 和过铝质特征 ($A/\text{CNK} = 1.01 \sim 1.21$); 具有相似的球粒陨石标准化稀土元素配分曲线并显示轻稀土富集、Eu 负异常 ($\delta\text{Eu} = 0.30 \sim 0.46$) 和在原始地幔标准化多元素图解上显示 Rb、Th、U 和 K 正异常, Ba、Nb、Ta、Sr、P 和 Ti 负异常; 具有富集的锆石 Hf 同位素组成, 其 $\varepsilon_{\text{Hf}}(t)$ 值为 $-5.0 \sim -1.4$ 和相应的两阶段 Hf 模式年龄为 $2.08 \sim 1.86$ Ga。这些地球化学特征共同反应似斑状花岗岩为壳源花岗岩, 并指示早期地壳的再造事件。结合前人发表的地球化学数据, 北山造山带南部前寒武纪基底经历了中元古代地壳新生事件和新元古代早期地壳再造事件, 花岗质岩石锆石 $\varepsilon_{\text{Hf}}(t)$ 值主要落在 $2.2 \sim 1.3$ Ga 地壳物质 Hf 同位素演化区内, 指示北山南部不存在太古代基底, 因此与具有太古代结晶基底的塔里木克拉通可能不具有构造亲缘性。

关键词: 新元古代; 花岗质岩石; 地壳再造; 北山造山带

中图分类号: P597

文献标志码: A

文章编号: 1009-6248(2024)06-0044-14

Age, Geochemistry and Geological Significance of an Early Neoproterozoic Porphyritic Granite in the Jianshanzi Area of the Beishan Orogenic Belt

WANG Biren^{1,2}, TENG Chao^{3,*}, BAI Xiangdong¹, GUAN Chengyao¹, YUAN Sihua¹, ZHANG Xiaofei⁴, YANG Xinjie³

(1. School of Earth Sciences, Institute of Disaster Prevention, Sanhe 065201, Hebei, China; 2. Hebei Key Laboratory of Earthquake Dynamics, Sanhe 065201, Hebei, China; 3. Cores and Samples Center of Natural Resources, China Geological Survey, Sanhe 065201, Hebei, China; 4. Development and Research Centre, China Geological Survey, Beijing 100037, China)

收稿日期: 2023-12-31; 修回日期: 2024-08-01; 责任编辑: 曹佰迪

基金项目: 廊坊市科学技术研究与发展计划自筹经费项目“三河市段甲岭-邦均断裂断层泥石英微形貌及其年代学研究”(2021013165), 中央高校基本科研业务费专项自主申报项目“北山微地块前寒武纪地层对比及其对构造亲缘性的制约”(ZY20215119)联合资助。

作者简介: 王必任(1985-), 男, 博士, 讲师, 主要从事构造地质学教学与区域地质研究。E-mail: 565985412@qq.com。

* 通讯作者: 滕超(1985-), 男, 硕士, 高级工程师, 主要从事基础地质调查与研究工作。E-mail: 275498009@qq.com。

Abstract: The geochronological and geochemical data of an early Neoproterozoic porphyritic granite in the Jianshanzi Area of the Beishan Orogenic Belt has been present. Combined with published geochemical data of contemporaneous granitic rocks, their magma sources and the tectonic affinity between the Precambrian basement in the southern Beishan and Tarim Craton are discussed. Two samples from the porphyritic granite have zircon U-Pb ages of (901 ± 5) Ma and (935 ± 3) Ma, respectively, indicating that it was formed during the early Neoproterozoic. Samples from the porphyritic granite contain K-feldspar phenocrysts with high SiO_2 contents ($70.41\% \sim 76.05\%$) and peraluminous characteristics ($A/\text{CNK}=1.01 \sim 1.21$), and exhibit similar chondrite-normalized REE patterns with LREE-enrichment and pronounced negative Eu anomalies ($\delta\text{Eu} = 0.30 \sim 0.46$), and show positive Rb, Th, U and K anomalies, negative Ba, Nb, Ta, Sr, P and Ti anomalies in the primitive mantle-normalized trace-element diagram, and have evolved zircon $\varepsilon_{\text{Hf}}(t)$ values of -5.0 to -1.4 and two-stage Hf model ages of $2.08 \sim 1.61$ Ga. All these geochemical characteristics suggest that the porphyritic granite is a typical crustal-derived granite, indicating an older crustal reworking event. Together with the reported data, the Precambrian basement of the southern Beishan experienced both Mesoproterozoic crustal growth and early Neoproterozoic crustal reworking events with the zircon $\varepsilon_{\text{Hf}}(t)$ values of granitic rocks plotting within the crustal evolution trend defined by $2.1 \sim 1.3$ Ga crustal material, indicating the absence of an Archean basement in the southern Beishan, and therefore it may not have tectonic affinity with the Tarim craton with an Archean crystalline basement.

Keywords: Neoproterozoic; granitic rocks; crustal reworking; Beishan Orogenic Belt

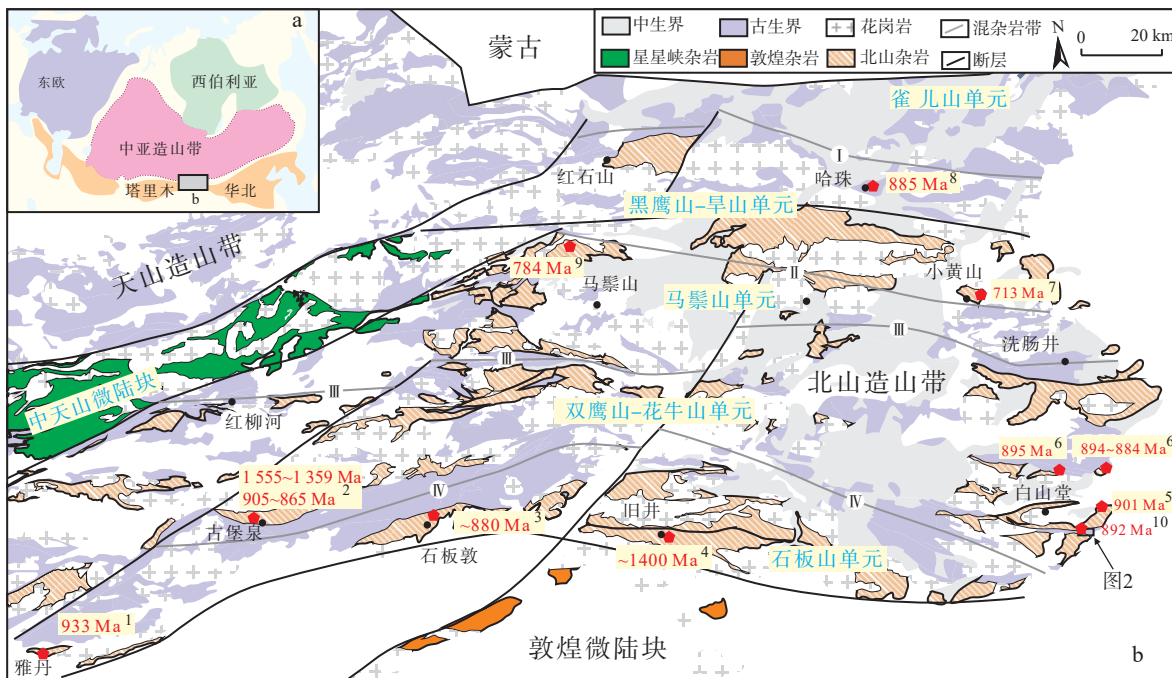
中亚造山带位于东欧克拉通、西伯利亚克拉通和塔里木–华北克拉通之间(图1a), 是世界上目前已知的发展历史最长、构造–岩浆作用最复杂的一条显生宙巨型增生造山带(Sengör et al., 1993; Windley et al., 2007; Xiao et al., 2010; 王文宝等, 2024; 吴妍蓉等, 2024), 带内分布着大小不等的前寒武纪微地块(Kröner et al., 2013; He et al., 2018; Zhou et al., 2018)。北山造山带位于中亚造山带中段南部, 是理解中亚造山带造山过程的关键地段(Xiao et al., 2010; Niu et al., 2021a, 2021b; 俞胜等, 2022; 戴鹏飞等, 2023)。早期研究认为该造山带不同构造单元分布着大量的前寒武纪基底, 即“北山杂岩”(左国朝等, 1990; Zuo et al., 1991; 何世平等, 2002; 杨合群等, 2008, 2009, 2010, 2012)。近年来, 一些前人认为的前寒武纪基底被锆石U-Pb年代学研究所否定(Song et al. 2013a, 2013b, 2013c, 2015, 2016; Zheng et al., 2018; 肖文交等, 2019; 霍宁等, 2022), 但北山地区确实存在前寒武纪岩石(梅华林等, 1999; 叶晓峰等, 2013; 姜洪颖等, 2013; Yuan et al., 2015; 贺振宇等, 2015; Liu et al., 2015; Ao et al., 2016; Soldner et al., 2019; 牛文超等, 2019; Wang et al., 2021a, 2021b; 李沅柏等, 2021; 卜涛等, 2022; Huang et al., 2022), 主要分布在红柳河–牛圈子–洗肠井缝合带以南, 即北山造山带南部(图1b)。然而, 关于前寒武纪基底起源的认识仍然缺少很好的

约束, 特别是与塔里木克拉通或敦煌微陆块(塔里木克拉通东缘)是否具有构造亲缘性(左国朝等, 1990, Zuo et al., 1991; 何世平等, 2002, 2005; 贺振宇等, 2015; Yuan et al., 2015; He et al., 2018; Wang et al., 2021b; Huang et al., 2022)。笔者报道了尖山子新元古代早期似斑状花岗岩的岩相学、年代学和地球化学数据, 分析了岩浆源区特征, 并结合已发表的岩浆岩数据, 讨论了前寒武纪基底与塔里木克拉通的亲缘性。

1 区域地质

北山造山带位于中亚造山带中段南部, 南为敦煌微陆块即塔里木克拉通的东缘, 北为蒙古古生代拼贴带, 西临东天山造山带, 东被巴丹吉林沙漠掩盖(图1b)(Zuo et al., 1991; Xiao et al., 2010)。北山造山带包括多个构造带及之间的构造单元, 以Xiao等(2010)的划分为代表, 其构造单元从北向南包括雀儿山、黑鹰山–旱山、马鬃山、双鹰山–花牛山、石板山等构造单元(图1b)。

早期研究认为北山造山带除了雀儿山构造单元外, 其他构造单元前寒武纪基底即“北山杂岩”广泛分布, 由中高级变质岩和浅变质沉积序列组成(左国朝等, 1990, Zuo et al., 1991; 杨合群等, 2008)。20世纪



蛇绿混杂岩带或裂谷带：I. 红石山构造带；II. 星星峡-石板井构造带；III. 红柳河-洗肠井构造带；IV. 柳园构造带。锆石U-Pb年龄：1. Yuan et al., 2015；2. 梅华林等, 1999; 叶晓峰等, 2013; Liu et al., 2015; Yuan et al., 2015; He et al., 2018; Soldner et al., 2019; Li et al., 2023; 3. 姜洪颖等, 2013; 4. 贺振宇等, 2015; Yuan et al., 2019; 5. Wang et al., 2021a; 6. Wang et al., 2021b; 7. Ao et al., 2016; 8. 牛文超等, 2019; 9. 卜涛等, 2022; 10. 李沅柏等, 2021

图1 中亚造山带构造位置图, 显示北山造山带的位置(a)和北山造山带北山杂岩及已知的前寒武纪岩石空间分布(b)
(据 Xiao et al., 2010; Wang et al., 2021b)

Fig. 1 (a) Simplified tectonic sketch map of the Central Asian Orogenic Belt showing the location of the Beishan Orogenic Belt and (b) distribution of the Beishan complex and the known Precambrian rocks in the Beishan Orogenic Belt

末至21世纪初, 前人研究依据变质变形、岩石组合和少量的全岩Sm-Nd等时线年龄、Ar-Ar年龄和单颗粒锆石U-Pb上交点年龄(主要获得2.9~1.6 Ga), 认为中高级变质岩形成时代为太古代—古元古代(李志琛, 1994; 桑海清等, 1997; 梅华林等, 1997; 魏学平等, 2000; 聂凤军等, 2004; 孙新春等, 2005), 依据区域岩石地层对比、与中高级变质岩变质差异, 认为浅变质沉积序列形成于中—新元古代(左国朝等, 1990, Zuo et al., 1991; 梅华林等, 1997; 杨合群等, 2008)。传统上认为北山造山带南部(红柳河-洗肠井蛇绿混杂岩带以南)前寒武纪基底具有塔里木克拉通或敦煌微陆块(塔里木克拉通的东端)的亲缘性(左国朝等, 1990, Zuo et al., 1991; 何世平等, 2002, 2005; 杨合群等, 2008, 2009, 2010, 2012)。

近年来, 地质学家对这些所谓的前寒武纪岩石进行了锆石U-Pb定年, 获得了不同的年龄数据, 但缺少太古代和古元古代的岩石。目前发现具有可靠年龄数据最老的岩石为出露在石板山构造单元约1400 Ma的旧井花岗质片麻岩(贺振宇等, 2015; Yuan et al.,

2019)和出露在双鹰山单元上与古堡泉超高压变质岩空间上共生的1555~1359 Ma花岗质片麻岩(He et al., 2018; Li et al., 2023), 并且一些所谓的前寒武纪变质岩已经被否定掉, 它们为古生代的俯冲增生杂岩或岩浆弧杂岩(Song et al., 2013a, 2013b, 2013c, 2015, 2016; Zheng et al., 2018)。因此, 北山造山带是否存在太古代—古元古代的岩石仍然不清楚(姜洪颖等, 2013; 贺振宇等, 2015; He et al., 2018)。

岩浆岩的地球化学特征, 特别是同位素特征, 可以指示源区的属性(贺振宇等, 2015; He et al., 2018)。论文报道了北山南部尖山子地区新元古代早期似斑状花岗岩, 结合已经发表的同时期花岗质岩石地球化学数据, 表征其源区特征, 并进行了前寒武纪基底亲缘性的探讨。

2 似斑状花岗岩及其样品采集

尖山子似斑状花岗岩位于北山造山带南部双鹰山-花牛山构造单元的东缘(图1b), 侵入到变质的北

山杂岩中，并被古生代岩浆岩侵入，后期与石炭纪地层呈断层接触（图2）。似斑状花岗岩，出露面积约10 km²，呈NWW-SEE展布。露头上，岩石呈黑灰色，发育肉红色钾长石斑晶，并且经历了韧性剪切变形（图3a、图3b）。本次工作采集了3件样品（TW1003, TW8837, YQ2224）（图2），所有样品呈似斑状结构，主要由斑晶和基质组成，斑晶为钾长石（10%~25%），多

自形，大小为5~10mm，基质为黑云母（5%~10%），石英（20%~25%）和长石（30%~40%，钾长石和斜长石近于相等）（图3a、图3b）。岩石经历韧性变形，石英矿物拉长定向排列或细粒化（图3b）。3件样品进行了主量元素和微量元素分析，两件样品（TW1003, TW8837）进行了锆石U-Pb测年，在锆石定年基础上，对样品TW1003开展了锆石Hf同位素分析。

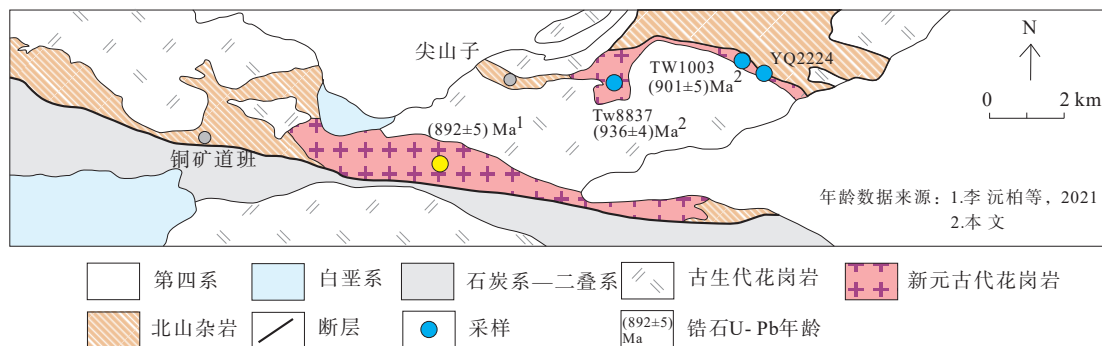


图2 北山造山带东缘尖山子地区地质简图及采样位置

Fig. 2 Sketch geological map and sampling location in the Jianshanzi area, eastern Beishan Orogenic Belt

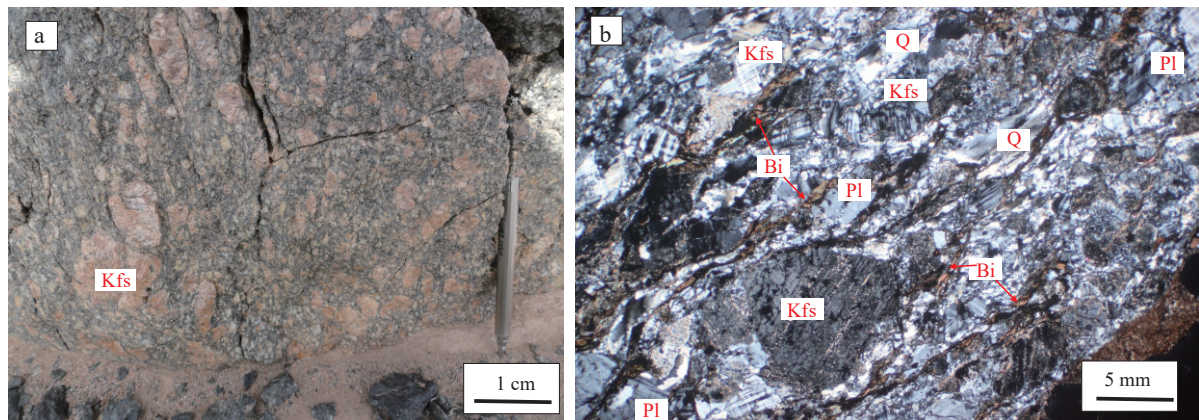


图3 尖山子似斑状花岗岩野外露头(a)和显微照片(b)

Fig. 3 (a) Field outcrop and (b) photomicrograph for the porphyritic granite in the Jianshanzi area

3 分析方法

样品主量元素和微量元素均在河北省区域地质矿产调查研究所实验室完成。主量元素采用X射线荧光光谱仪，分析精度优于5%。微量元素采用X-Serises 2电感耦合等离子体质谱ICP-MS分析方法，精度优于5%。

锆石分选、制靶、阴极发光在河北省区域地质矿产调查研究所实验室完成。锆石U-Pb同位素定年在

天津地质矿产研究所利用LA-ICP-MS Agilent 7500a仪器分析。本次实验室采用的激光束斑直径为50 μm，以氦气作为剥蚀物质的载气。LA-ICP-MS分析方法见李怀坤等（2010）相关描述。测试数据年龄值误差均为1σ，计算处理采用Isoplot 3.0程序。

锆石Hf同位素分析在北京锆石领航科技有限公司激光剥蚀多接收器电感耦合等离子体质谱仪上完成。激光进样系统为NWR 213nm固体激光器，分析系统为多接收等离子体质谱仪（NEPTUNE plus）。实验中采用¹⁷⁹Hf/¹⁷⁷Hf=0.7325对Hf同位素比值进行指

数归一化质量歧视校正,采用 $^{173}\text{Yb}/^{172}\text{Yb} = 1.352\,74$ 对Yb同位素比值进行指数归一化质量歧视校正。测试过程中采用GJ-1作为标样,测量 $^{176}\text{Hf}/^{177}\text{Hf}$ 平均值为0.282 011。

4 分析结果

4.1 锆石U-Pb年龄

样品TW1003锆石U-Pb年龄数据见表1和图4。

锆石多呈自形,长为80~120 μm,宽度为50~80 μm,长宽比接近2:1。阴极发光图像显示锆石具有明显的振荡环带,显示岩浆成因的结构特征,此外部分锆石具有核幔结构(图4a)。锆石一共分析了32个点(图4b),9个分析点位于锆石核部,其中两个分析点谐和性差,7个分析点落在谐和线附近, $^{206}\text{Pb}/^{238}\text{U}$ 年龄介于1 415~951 Ma,代表了捕获或残留锆石年龄。

23个分析点无核部结构或位于幔部,其中19个分析点集中分布在谐和线上, $^{206}\text{Pb}/^{238}\text{U}$ 年龄平均年龄为

表1 尖山子似斑状花岗岩样品TW1003锆石LA-ICP-MS U-Pb年龄分析数据

Tab. 1 Zircon LA-ICP-MS U-Pb data for the sample TW1003 from the porphyritic granite in the Jianshanzi area

| 点号 | 含量(10^{-6}) | | | 同位素比值 | | | | | | 年龄(Ma) | | | | | | | |
|------------|-----------------|-----|-------|-----------------------------------|-----------|----------------------------------|-----------|----------------------------------|-----------|-----------------------------------|-----------|-----------------------------------|-----------|----------------------------------|-----------|----------------------------------|-----------|
| | Pb | Th | U | $^{207}\text{Pb}/^{206}\text{Pb}$ | 1σ | $^{207}\text{Pb}/^{235}\text{U}$ | 1σ | $^{206}\text{Pb}/^{238}\text{U}$ | 1σ | $^{208}\text{Pb}/^{232}\text{Th}$ | 1σ | $^{207}\text{Pb}/^{206}\text{Pb}$ | 1σ | $^{207}\text{Pb}/^{235}\text{U}$ | 1σ | $^{206}\text{Pb}/^{238}\text{U}$ | 1σ |
| TW1003 | | | | | | | | | | | | | | | | | |
| TW1003-1 | 126 | 220 | 719 | 0.0713 | 0.0023 | 1.4571 | 0.0456 | 0.1474 | 0.0020 | 0.0494 | 0.0019 | 966 | 67 | 913 | 19 | 886 | 11 |
| TW1003-2 | 127 | 91 | 1 024 | 0.0666 | 0.0018 | 1.2808 | 0.0355 | 0.1385 | 0.0018 | 0.0472 | 0.0030 | 833 | 56 | 837 | 16 | 836 | 10 |
| TW1003-3* | 302 | 200 | 1 583 | 0.0814 | 0.0025 | 1.9176 | 0.0526 | 0.1700 | 0.0021 | 0.1138 | 0.0041 | 1 231 | 65 | 1 087 | 18 | 1 012 | 12 |
| TW1003-4* | 1 361 | 722 | 2 152 | 0.3820 | 0.0091 | 8.0679 | 0.3240 | 0.1502 | 0.0042 | 0.3970 | 0.0185 | 3 840 | 36 | 2 239 | 36 | 902 | 23 |
| TW1003-5 | 194 | 263 | 1 199 | 0.0696 | 0.0018 | 1.4317 | 0.0401 | 0.1481 | 0.0022 | 0.0624 | 0.0041 | 917 | 52 | 902 | 17 | 891 | 12 |
| TW1003-6 | 130 | 70 | 1 036 | 0.0687 | 0.0016 | 1.4336 | 0.0425 | 0.1505 | 0.0030 | 0.0458 | 0.0022 | 889 | 50 | 903 | 18 | 904 | 17 |
| TW1003-7 | 129 | 431 | 643 | 0.0726 | 0.0020 | 1.5261 | 0.0511 | 0.1508 | 0.0027 | 0.0460 | 0.0014 | 1 011 | 56 | 941 | 21 | 905 | 15 |
| TW1003-8* | 104 | 213 | 452 | 0.0756 | 0.0023 | 1.8682 | 0.0597 | 0.1787 | 0.0026 | 0.0584 | 0.0019 | 1 087 | 62 | 1 070 | 21 | 1 060 | 14 |
| TW1003-9 | 116 | 359 | 592 | 0.0696 | 0.0019 | 1.4392 | 0.0412 | 0.1494 | 0.0021 | 0.0456 | 0.0012 | 917 | 54 | 905 | 17 | 898 | 12 |
| TW1003-10 | 128 | 106 | 957 | 0.0693 | 0.0017 | 1.4330 | 0.0379 | 0.1488 | 0.0018 | 0.0503 | 0.0018 | 907 | 55 | 903 | 16 | 894 | 10 |
| TW1003-11* | 199 | 591 | 844 | 0.0754 | 0.0019 | 1.6734 | 0.0494 | 0.1590 | 0.0023 | 0.0554 | 0.0017 | 1 080 | 50 | 998 | 19 | 951 | 13 |
| TW1003-12 | 248 | 126 | 1 819 | 0.0770 | 0.0016 | 1.6131 | 0.0425 | 0.1501 | 0.0024 | 0.0994 | 0.0041 | 1 120 | 43 | 975 | 17 | 902 | 13 |
| TW1003-13 | 151 | 92 | 1 202 | 0.0671 | 0.0014 | 1.4167 | 0.0310 | 0.1520 | 0.0021 | 0.0502 | 0.0014 | 840 | 43 | 896 | 13 | 912 | 12 |
| TW1003-14 | 101 | 69 | 794 | 0.0675 | 0.0014 | 1.4265 | 0.0318 | 0.1516 | 0.0020 | 0.0503 | 0.0016 | 854 | 44 | 900 | 13 | 910 | 11 |
| TW1003-15 | 468 | 827 | 1 665 | 0.0899 | 0.0021 | 2.7197 | 0.0699 | 0.2163 | 0.0031 | 0.0742 | 0.0019 | 1 433 | 39 | 1 334 | 19 | 1 262 | 17 |
| TW1003-16 | 98 | 84 | 711 | 0.0695 | 0.0024 | 1.4644 | 0.0617 | 0.1499 | 0.0022 | 0.0651 | 0.0076 | 922 | 72 | 916 | 25 | 900 | 13 |
| TW1003-17* | 605 | 257 | 1 807 | 0.1891 | 0.0094 | 4.4913 | 0.2548 | 0.1631 | 0.0032 | 0.4163 | 0.0262 | 2 744 | 82 | 1 729 | 47 | 974 | 18 |
| TW1003-18 | 140 | 59 | 1 105 | 0.0671 | 0.0015 | 1.4159 | 0.0327 | 0.1511 | 0.0020 | 0.0522 | 0.0016 | 839 | 48 | 896 | 14 | 907 | 11 |
| TW1003-19* | 301 | 91 | 1 565 | 0.1267 | 0.0046 | 2.4865 | 0.1035 | 0.1387 | 0.0018 | 0.5338 | 0.0471 | 2 054 | 64 | 1 268 | 30 | 837 | 10 |
| TW1003-20 | 70 | 196 | 372 | 0.0684 | 0.0016 | 1.4270 | 0.0332 | 0.1500 | 0.0019 | 0.0464 | 0.0012 | 880 | 48 | 900 | 14 | 901 | 11 |
| TW1003-21 | 97 | 97 | 714 | 0.0655 | 0.0014 | 1.3836 | 0.0313 | 0.1512 | 0.0019 | 0.0466 | 0.0014 | 791 | 46 | 882 | 13 | 908 | 10 |
| TW1003-22 | 205 | 172 | 1 221 | 0.0892 | 0.0028 | 1.8853 | 0.0642 | 0.1500 | 0.0019 | 0.1024 | 0.0050 | 1 409 | 92 | 1 076 | 23 | 901 | 10 |
| TW1003-23 | 82 | 258 | 418 | 0.0673 | 0.0016 | 1.4125 | 0.0377 | 0.1502 | 0.0024 | 0.0480 | 0.0014 | 856 | 48 | 894 | 16 | 902 | 13 |
| TW1003-24 | 158 | 102 | 1 221 | 0.0663 | 0.0015 | 1.3876 | 0.0355 | 0.1498 | 0.0022 | 0.0471 | 0.0015 | 815 | 49 | 884 | 15 | 900 | 12 |
| TW1003-25* | 544 | 999 | 1 507 | 0.0934 | 0.0025 | 3.1789 | 0.0964 | 0.2424 | 0.0036 | 0.0757 | 0.0025 | 1 496 | 45 | 1 452 | 23 | 1 399 | 18 |
| TW1003-26* | 146 | 73 | 1 033 | 0.0695 | 0.0016 | 1.5503 | 0.0365 | 0.1600 | 0.0023 | 0.0613 | 0.0023 | 922 | 47 | 951 | 15 | 957 | 13 |
| TW1003-27 | 174 | 203 | 1 203 | 0.0701 | 0.0016 | 1.4758 | 0.0350 | 0.1507 | 0.0018 | 0.0508 | 0.0018 | 931 | 46 | 921 | 14 | 905 | 10 |
| TW1003-28 | 182 | 104 | 1 304 | 0.0723 | 0.0016 | 1.5195 | 0.0343 | 0.1512 | 0.0020 | 0.0730 | 0.0025 | 994 | 46 | 938 | 14 | 908 | 11 |
| TW1003-29 | 143 | 106 | 1 084 | 0.0687 | 0.0015 | 1.4335 | 0.0359 | 0.1491 | 0.0018 | 0.0561 | 0.0043 | 900 | 72 | 903 | 15 | 896 | 10 |
| TW1003-30* | 290 | 516 | 902 | 0.0874 | 0.0017 | 2.9888 | 0.0637 | 0.2455 | 0.0030 | 0.0716 | 0.0016 | 1 369 | 37 | 1 405 | 16 | 1 415 | 16 |
| TW1003-31 | 87 | 202 | 508 | 0.0690 | 0.0016 | 1.4469 | 0.0353 | 0.1506 | 0.0020 | 0.0450 | 0.0012 | 898 | 48 | 909 | 15 | 904 | 11 |
| TW1003-32 | 112 | 74 | 849 | 0.0689 | 0.0017 | 1.4329 | 0.0369 | 0.1492 | 0.0019 | 0.0482 | 0.0015 | 898 | 45 | 903 | 15 | 896 | 11 |

注: *表示锆石核部点位。

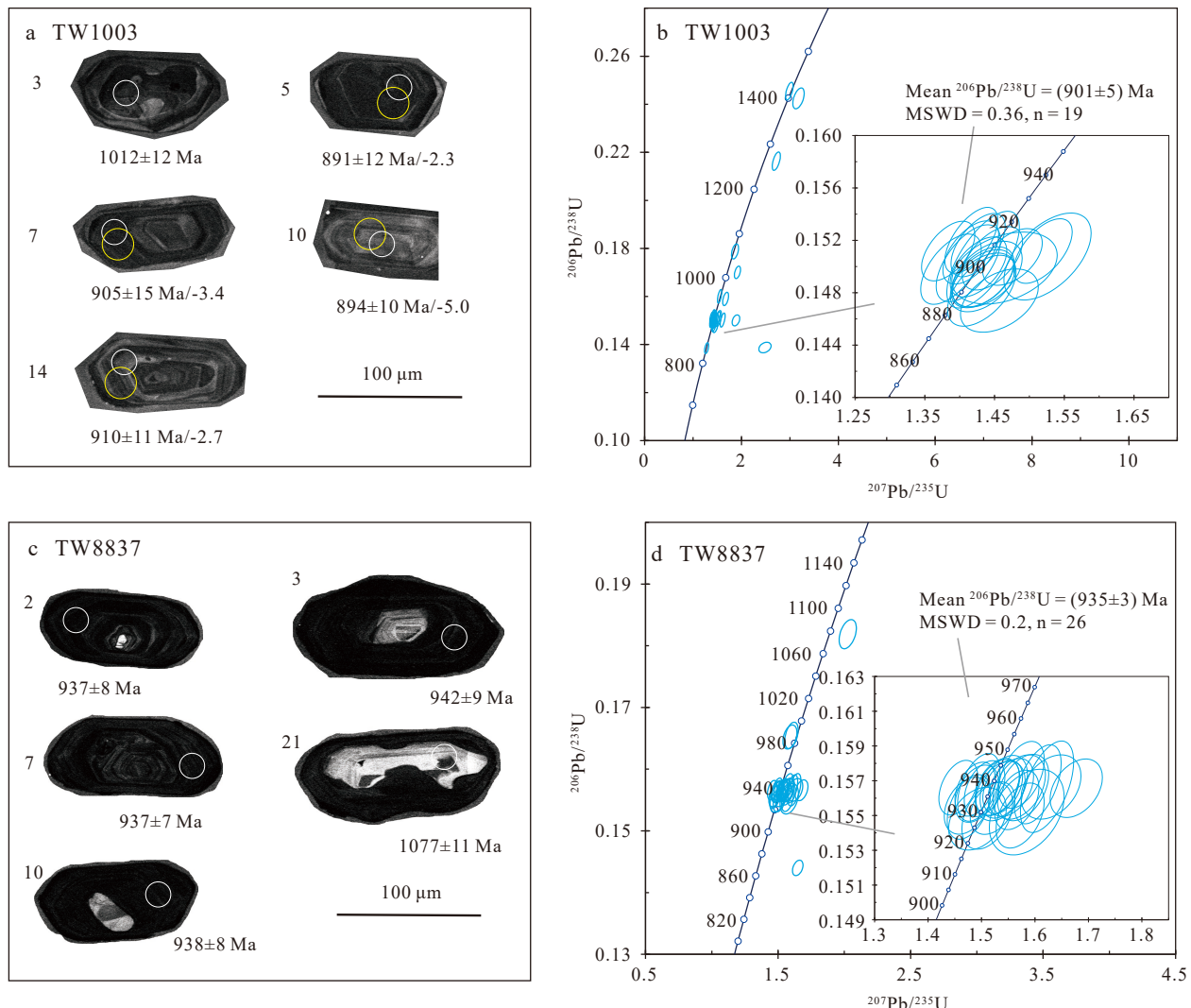


图 a 中白色小圆圈为年龄测点，黄色大圆圈为 Hf 同位素测点，年龄和 $\epsilon_{\text{Hf}}(t)$ 值标注在正下方

图4 尖山子似斑状花岗岩锆石阴极发光(a、c)及锆石 U-Pb 谱和图(b、d)

Fig. 4 (a, c) Cathodoluminescence images of representative zircon grains and (b, d) zircon U-Pb concordia diagrams from the porphyritic granite in the Jianshanzi area

(901±5) Ma, 代表了样品 TW1003 的结晶年龄; 另外 3 个分析点谐和性差和 1 个分析点落在谐和曲线上, 但 $^{206}\text{Pb}/^{238}\text{U}$ 年龄为 836 Ma 且与结晶年龄相比明显偏年轻, 这些分析点可能与锆石重结晶或 Pb 同位素丢失有关(王梓桐等, 2022; 牛腾等, 2023)。

样品 TW8837 锆石 U-Pb 年龄数据见表 2 和图 4。锆石多呈自形, 长度为 80~150 μm, 宽度为 50~90 μm, 长宽比接近 1.5 : 1。阴极发光图像显示锆石颜色比较深, 多呈灰黑色, 但振荡环带清楚, 显示岩浆成因的结构特征, 此外部分锆石具有核幔结构(图 4c)。锆石一共分析了 30 个点, 谐和图见图 4d。3 个分析点位于锆石核部, 数据落在谐和线附近, $^{206}\text{Pb}/^{238}\text{U}$ 年龄介于 1 077~

986 Ma, 代表了捕获或残留锆石年龄。27 个分析点无核部结构或位于幔部, 1 个分析点偏离谐和曲线, 其余 26 个分析点落在谐和曲线上, 年龄集中分布, $^{206}\text{Pb}/^{238}\text{U}$ 年龄平均年龄为 (935±3) Ma, 代表了样品 TW8837 的结晶年龄。

4.2 锆石 Hf 同位素

样品 TW1003 选择谐和年龄的结晶锆石进行 Hf 同位素分析, 并用 $^{206}\text{Pb}/^{238}\text{U}$ 年龄平均值 (901±5) Ma 计算 $\epsilon_{\text{Hf}}(t)$ 值和两阶段 Hf 模式年龄 $T_{\text{DM}2}$ (DM 代表亏损地幔)。Hf 同位素的组成见表 3, 结果与北山造山带南部报道的花岗质岩石 Hf 同位素组成类似(图 5; 姜洪颖等, 2013; 叶晓峰等, 2013; Liu et al., 2015; Yuan et

表2 尖山子似斑状花岗岩样品 TW8837 锆石 LA-ICP-MS U-Pb 年龄分析数据

Tab. 2 Zircon LA-ICP-MS U-Pb data for the sample TW8837 from the porphyritic granite in the Jianshanzi area

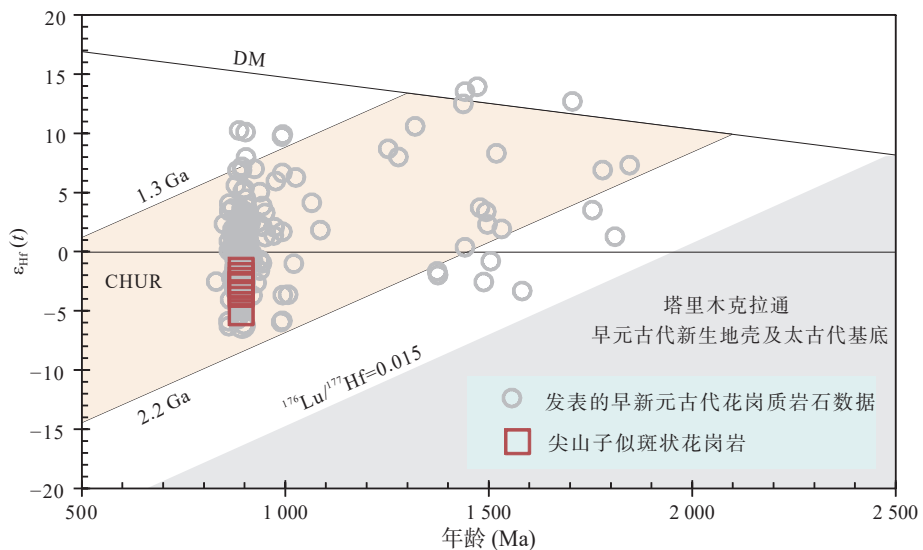
| 点号 | 含量 (10^{-6}) | | | | | | | | | | 同位素比值 | | | | | | 年龄 (Ma) | | | | | |
|------------|------------------|-------|-------|-----------------------------------|------------|----------------------------------|------------|----------------------------------|------------|-----------------------------------|------------|-----------------------------------|------------|----------------------------------|------------|----------------------------------|------------|--|--|--|--|--|
| | Pb | Th | U | $^{207}\text{Pb}/^{206}\text{Pb}$ | 1 σ | $^{207}\text{Pb}/^{235}\text{U}$ | 1 σ | $^{206}\text{Pb}/^{238}\text{U}$ | 1 σ | $^{208}\text{Pb}/^{232}\text{Th}$ | 1 σ | $^{207}\text{Pb}/^{206}\text{Pb}$ | 1 σ | $^{207}\text{Pb}/^{235}\text{U}$ | 1 σ | $^{206}\text{Pb}/^{238}\text{U}$ | 1 σ | | | | | |
| TW8837 | | | | | | | | | | | | | | | | | | | | | | |
| TW8837-1 | 578 | 565 | 2 424 | 0.072 1 | 0.001 8 | 1.570 4 | 0.040 1 | 0.156 6 | 0.001 5 | 0.054 8 | 0.001 6 | 989 | 19 | 959 | 16 | 938 | 8 | | | | | |
| TW8837-2 | 392 | 565 | 1 343 | 0.070 8 | 0.001 8 | 1.535 4 | 0.037 8 | 0.156 4 | 0.001 4 | 0.047 9 | 0.001 1 | 950 | 56 | 945 | 15 | 937 | 8 | | | | | |
| TW8837-3 | 2 373 | 4 494 | 5 527 | 0.072 2 | 0.001 7 | 1.574 7 | 0.034 9 | 0.157 3 | 0.001 6 | 0.047 7 | 0.001 1 | 991 | 48 | 960 | 14 | 942 | 9 | | | | | |
| TW8837-4 | 1 354 | 2 073 | 4 069 | 0.070 8 | 0.001 4 | 1.539 7 | 0.030 4 | 0.156 6 | 0.001 2 | 0.050 2 | 0.001 0 | 950 | 41 | 946 | 12 | 938 | 7 | | | | | |
| TW8837-5 | 792 | 1 023 | 3 056 | 0.067 0 | 0.001 4 | 1.456 6 | 0.029 7 | 0.156 6 | 0.001 3 | 0.046 9 | 0.000 9 | 835 | 43 | 913 | 12 | 938 | 7 | | | | | |
| TW8837-6 | 1 623 | 2 081 | 5 514 | 0.082 5 | 0.001 8 | 1.648 8 | 0.032 9 | 0.144 0 | 0.001 0 | 0.055 7 | 0.001 1 | 1 258 | 42 | 989 | 13 | 867 | 6 | | | | | |
| TW8837-7 | 641 | 530 | 3 129 | 0.068 5 | 0.001 4 | 1.487 9 | 0.030 7 | 0.156 5 | 0.001 3 | 0.049 0 | 0.001 2 | 883 | 43 | 925 | 13 | 937 | 7 | | | | | |
| TW8837-8 | 409 | 285 | 1 947 | 0.070 4 | 0.001 6 | 1.530 3 | 0.033 6 | 0.156 6 | 0.001 3 | 0.060 7 | 0.001 6 | 939 | 46 | 943 | 13 | 938 | 7 | | | | | |
| TW8837-9 | 494 | 375 | 2 598 | 0.071 5 | 0.001 6 | 1.554 7 | 0.034 9 | 0.156 6 | 0.001 4 | 0.041 8 | 0.001 1 | 972 | 47 | 952 | 14 | 938 | 8 | | | | | |
| TW8837-10 | 1 555 | 2 353 | 4 238 | 0.074 4 | 0.002 0 | 1.630 1 | 0.045 8 | 0.156 6 | 0.001 5 | 0.056 3 | 0.002 2 | 1 054 | 54 | 982 | 18 | 938 | 8 | | | | | |
| TW8837-11 | 986 | 1 372 | 3 002 | 0.072 6 | 0.001 8 | 1.577 8 | 0.039 2 | 0.156 6 | 0.001 6 | 0.052 7 | 0.001 2 | 1 003 | 52 | 962 | 15 | 938 | 9 | | | | | |
| TW8837-12 | 514 | 430 | 2 269 | 0.070 9 | 0.001 7 | 1.541 6 | 0.036 2 | 0.156 7 | 0.001 5 | 0.056 5 | 0.001 5 | 955 | 53 | 947 | 14 | 938 | 8 | | | | | |
| TW8837-13 | 607 | 414 | 2 654 | 0.073 9 | 0.001 7 | 1.622 6 | 0.040 6 | 0.156 7 | 0.002 2 | 0.068 1 | 0.002 4 | 1 039 | 48 | 979 | 16 | 938 | 12 | | | | | |
| TW8837-14 | 927 | 1 433 | 2 810 | 0.074 1 | 0.001 7 | 1.605 2 | 0.035 8 | 0.156 8 | 0.001 9 | 0.047 5 | 0.001 1 | 1 043 | 52 | 972 | 14 | 939 | 10 | | | | | |
| TW8837-15 | 443 | 288 | 2 252 | 0.068 8 | 0.001 5 | 1.494 9 | 0.032 3 | 0.156 6 | 0.001 6 | 0.051 7 | 0.001 2 | 892 | 76 | 928 | 13 | 938 | 9 | | | | | |
| TW8837-16 | 818 | 578 | 4 164 | 0.069 3 | 0.001 4 | 1.505 7 | 0.031 1 | 0.156 5 | 0.001 3 | 0.046 6 | 0.001 0 | 909 | 43 | 933 | 13 | 938 | 7 | | | | | |
| TW8837-17 | 498 | 321 | 2 396 | 0.072 4 | 0.001 6 | 1.565 9 | 0.034 0 | 0.155 9 | 0.001 4 | 0.057 3 | 0.001 4 | 998 | 43 | 957 | 13 | 934 | 8 | | | | | |
| TW8837-18 | 600 | 552 | 2 580 | 0.070 4 | 0.001 6 | 1.529 4 | 0.033 8 | 0.156 6 | 0.001 3 | 0.051 0 | 0.001 2 | 943 | 46 | 942 | 14 | 938 | 7 | | | | | |
| TW8837-19 | 507 | 431 | 2 290 | 0.068 8 | 0.001 6 | 1.491 5 | 0.033 3 | 0.156 3 | 0.001 3 | 0.050 5 | 0.001 3 | 894 | 42 | 927 | 14 | 936 | 7 | | | | | |
| TW8837-20 | 588 | 463 | 2 517 | 0.077 2 | 0.001 8 | 1.677 2 | 0.040 0 | 0.156 6 | 0.001 4 | 0.057 1 | 0.001 4 | 1 125 | 48 | 1 000 | 15 | 938 | 8 | | | | | |
| TW8837-21* | 646 | 468 | 2 250 | 0.080 0 | 0.001 9 | 2.026 1 | 0.052 9 | 0.181 9 | 0.001 9 | 0.074 7 | 0.001 8 | 1 198 | 46 | 1 124 | 18 | 1 077 | 11 | | | | | |
| TW8837-22 | 477 | 314 | 2 492 | 0.068 2 | 0.001 6 | 1.473 5 | 0.035 3 | 0.155 6 | 0.001 3 | 0.051 3 | 0.001 5 | 876 | 48 | 920 | 14 | 932 | 7 | | | | | |
| TW8837-23 | 628 | 985 | 1 916 | 0.070 5 | 0.001 6 | 1.520 8 | 0.034 2 | 0.155 4 | 0.001 2 | 0.048 7 | 0.001 0 | 943 | 45 | 939 | 14 | 931 | 7 | | | | | |
| TW8837-24 | 463 | 644 | 1 481 | 0.069 5 | 0.002 0 | 1.492 5 | 0.044 0 | 0.154 8 | 0.001 5 | 0.053 4 | 0.001 2 | 915 | 58 | 927 | 18 | 928 | 8 | | | | | |
| TW8837-25 | 486 | 456 | 2 299 | 0.068 5 | 0.001 5 | 1.476 5 | 0.033 2 | 0.155 5 | 0.001 5 | 0.048 7 | 0.001 1 | 883 | 44 | 921 | 14 | 932 | 8 | | | | | |
| TW8837-26 | 491 | 383 | 2 174 | 0.074 1 | 0.002 6 | 1.584 6 | 0.057 1 | 0.155 2 | 0.002 0 | 0.067 4 | 0.003 1 | 1 044 | 75 | 964 | 22 | 930 | 11 | | | | | |
| TW8837-27 | 568 | 327 | 2 975 | 0.073 1 | 0.001 6 | 1.572 3 | 0.036 8 | 0.155 0 | 0.001 5 | 0.063 1 | 0.001 9 | 1 017 | 44 | 959 | 15 | 929 | 9 | | | | | |
| TW8837-28 | 369 | 432 | 1 584 | 0.070 4 | 0.001 8 | 1.510 8 | 0.038 8 | 0.155 0 | 0.001 6 | 0.047 2 | 0.001 3 | 939 | 52 | 935 | 16 | 929 | 9 | | | | | |
| TW8837-29* | 481 | 467 | 1 812 | 0.070 0 | 0.001 8 | 1.601 7 | 0.041 2 | 0.165 5 | 0.001 7 | 0.062 2 | 0.001 8 | 928 | 55 | 971 | 16 | 987 | 10 | | | | | |
| TW8837-30* | 419 | 207 | 2 163 | 0.069 5 | 0.001 9 | 1.590 0 | 0.043 1 | 0.165 2 | 0.001 6 | 0.067 3 | 0.002 6 | 922 | 56 | 966 | 17 | 986 | 9 | | | | | |

注: *表示锆石核部点位。

表3 尖山子似斑状花岗岩样品 TW1003 锆石 Hf 同位素组成

Tab. 3 Zircon Hf-isotope compositions for the sample TW1003 from the porphyritic granite in the Jianshanzi area

| 点号 | $^{176}\text{Yb}/^{177}\text{Hf}$ | 2 σ | $^{176}\text{Lu}/^{177}\text{Hf}$ | 2 σ | $^{176}\text{Hf}/^{177}\text{Hf}$ | 2 σ | 年龄 (Ma) | $(^{176}\text{Hf}/^{177}\text{Hf})_i$ | $\epsilon_{\text{Hf}}(0)$ | $\epsilon_{\text{Hf}}(t)$ | T_{DM} (Ma) | $T_{\text{DM}2}$ (Ma) | $f_{\text{Lu/Hf}}$ |
|-----------|-----------------------------------|------------|-----------------------------------|------------|-----------------------------------|------------|------------|---------------------------------------|---------------------------|---------------------------|-------------------------|--------------------------|--------------------|
| TW1003-5 | 0.054 984 | 0.000 289 | 0.001 418 | 0.000 007 | 0.282 170 | 0.000 025 | 901 | 0.282 146 | -21.3 | -2.3 | 1 544 | 1 916 | -0.96 |
| TW1003-6 | 0.050 315 | 0.000 471 | 0.001 302 | 0.000 012 | 0.282 139 | 0.000 023 | 901 | 0.282 117 | -22.4 | -3.3 | 1 582 | 1 980 | -0.96 |
| TW1003-7 | 0.037 520 | 0.000 372 | 0.000 998 | 0.000 010 | 0.282 130 | 0.000 023 | 901 | 0.282 113 | -22.7 | -3.4 | 1 582 | 1 988 | -0.97 |
| TW1003-9 | 0.087 226 | 0.001 205 | 0.002 261 | 0.000 024 | 0.282 195 | 0.000 021 | 901 | 0.282 157 | -20.4 | -1.9 | 1 543 | 1 891 | -0.93 |
| TW1003-10 | 0.091 361 | 0.001 105 | 0.002 329 | 0.000 026 | 0.282 108 | 0.000 022 | 901 | 0.282 068 | -23.5 | -5.0 | 1 672 | 2 087 | -0.93 |
| TW1003-13 | 0.071 769 | 0.001 814 | 0.001 842 | 0.000 037 | 0.282 167 | 0.000 026 | 901 | 0.282 136 | -21.4 | -2.6 | 1 566 | 1 938 | -0.94 |
| TW1003-14 | 0.080 789 | 0.000 700 | 0.002 134 | 0.000 025 | 0.282 169 | 0.000 023 | 901 | 0.282 133 | -21.3 | -2.7 | 1 575 | 1 944 | -0.94 |
| TW1003-16 | 0.064 744 | 0.000 391 | 0.001 682 | 0.000 006 | 0.282 198 | 0.000 025 | 901 | 0.282 170 | -20.3 | -1.4 | 1 514 | 1 861 | -0.95 |



图中表示出了北山造山带南部新元古代早期花岗质岩石锆石 Hf 同位素; 数据来自叶晓峰等(2013)、
姜洪颖等(2013)、Liu 等(2015)、Yuan 等(2015)和 Wang 等(2021b)

图5 尖山子似斑状花岗岩样品 TW1003 锆石 $\epsilon_{\text{Hf}}(t)$ -年龄(Ma)图

Fig. 5 The zircon $\epsilon_{\text{Hf}}(t)$ versus age plot for the sample TW1003 from the porphyritic granite in the Jianshanzi area

al., 2015; Wang et al., 2021b)。

TW1003 样品 8 个分析点锆石 $^{176}\text{Lu}/^{177}\text{Hf}$ 值为 0.282 068~0.282 170, $\epsilon_{\text{Hf}}(t)$ 值为 -5.0~−1.4, T_{DM} 年龄值为 2.08~1.86 Ga。

4.3 主量和微量元素

尖山子 3 件似斑状花岗岩样品的主量和微量元素见表 4, 结果与李沅柏等(2021)报道的该岩体数据, 以及北山造山带南部已经发表的花岗质岩石地球化学特征类似(图 6、图 7)(姜洪颖等, 2013; 叶晓峰等, 2013; Liu et al., 2015; Yuan et al., 2015; Wang et al., 2021b)。样品 SiO_2 (70.41%~76.05%), K_2O (5.13%~5.33%) 的含量较高, Al_2O_3 (12.66%~14.25%), Na_2O (2.36%~2.53%) 和 CaO (1.25%~1.39%) 含量中等, MgO 含量偏低。样品 Rb 含量为 130.66×10^{-6} ~ 294.88×10^{-6} , Rb/Sr 值 (1.12~2.48) 相对较高。在 TAS 图上, 样品落在亚碱性花岗岩或接近亚碱性花岗闪长岩区(图 6a), 属于钙碱性或接近高钾钙碱性系列(图 6b)。这些样品显示过铝质特征, A/CNK 值 [$\text{Al}_2\text{O}_3/(\text{CaO} + \text{Na}_2\text{O} + \text{K}_2\text{O})$ 摩尔数比值] 为 1.01~1.21(图 6c)。

样品稀土总量为 138.47×10^{-6} ~ 362.78×10^{-6} , 并显示相似的球粒陨石稀土元素配分曲线(图 7a)。配分曲线向右倾斜, 显示轻稀土与重稀土的分离特征(La/Yb)_N 值为 7.17~10.79, 以及明显的 Eu 负异常($\delta\text{Eu} = 0.30 \sim 0.46$)(图 7a)。在原始地幔微量元素配分图解上, 这些样品显示 Rb、Th、U 和 K 正异常, 以及 Ba、Nb、Ta、Sr、

P 和 Ti 负异常(图 7b)。

5 讨论

5.1 新元古代早期地壳再造事件

尖山子似斑状花岗岩位于北山造山带南部东缘, 本次获得两件样品锆石 U-Pb 年龄分别为 (901±5) Ma, (935±3) Ma, 另外李沅柏等(2021)报道一件锆石 U-Pb 年龄为 (892±5) Ma, 表明该岩体形成时间为新元古代早期。同时期的岩浆事件在北山造山带南部发育(图 1b), 包括双鹰山-花牛山构造单元古堡泉片麻状花岗岩和变质基性岩(900~865 Ma; 梅华林等, 1999; 叶晓峰等, 2013; Liu et al., 2015; Yuan et al., 2015; Soldner et al., 2019)、东黑尖山花岗质片麻岩(895±4 Ma; Wang et al., 2021b)、石峡麻棱岩化花岗岩和二长岩(894~884 Ma; Wang et al., 2021b)、大湾城玄武岩(901±10 Ma; Wang et al., 2021a), 以及石板山构造单元雅丹片麻状花岗岩(933±2 Ma; Yuan et al., 2015)、白墩子片麻状花岗岩和石板敦斜长角闪岩(~880 Ma; 姜洪颖等, 2013)。这表明北山造山带南部广泛发育新元古代早期构造-岩浆事件。

上述新元古代花岗质岩石属于高钾钙碱性系列至钾玄岩系列, 显示偏铝质至过铝质的特征(图 6), 具有相似的稀土元素配分曲线并显示轻稀土富集、Eu 负异常的特征(图 7a), 以及在微量元素地球化学配分

表4 尖山子似斑状花岗岩样品主量(%)和微量元素(10^{-6})组成Tab. 4 Major (%) and trace element (10^{-6}) compositions for samples from the porphyritic granite in the Jianshanzi area

| 样号 | TW1003 | YQ2224 | TW8837 | 样号 | TW1003 | YQ2224 | TW8837 |
|---|--------|--------|--------|----------------------|--------|--------|--------|
| SiO ₂ | 76.05 | 72.01 | 70.41 | Y | 32.27 | 38.96 | 45.02 |
| Al ₂ O ₃ | 12.66 | 14.20 | 14.25 | Σ REE | 138.47 | 261.00 | 362.78 |
| TiO ₂ | 0.09 | 0.52 | 0.55 | (La/Yb) _N | 7.17 | 8.41 | 10.79 |
| Fe ₂ O ₃ ^t | 0.76 | 3.21 | — | δ Eu | 0.46 | 0.32 | 0.30 |
| Fe ₂ O ₃ | — | — | 1.48 | Li | 8.94 | 12.50 | 23.14 |
| FeO | — | — | 1.95 | Be | 1.35 | 2.57 | 2.86 |
| CaO | 1.39 | 1.25 | 1.30 | Sc | 5.41 | 10.10 | 8.83 |
| MgO | 0.47 | 0.85 | 1.11 | V | 9.51 | 40.64 | 53.43 |
| K ₂ O | 5.33 | 5.13 | 5.23 | Cr | 6.87 | 7.88 | 19.22 |
| Na ₂ O | 2.53 | 2.36 | 2.48 | Co | 66.15 | 64.20 | 5.97 |
| MnO | 0.04 | 0.03 | 0.04 | Ni | 3.20 | 4.82 | 6.94 |
| P ₂ O ₅ | 0.06 | 0.05 | 0.06 | Cu | 4.48 | 5.66 | 19.92 |
| LOI | 0.83 | 0.36 | 1.01 | Zn | 10.75 | 46.32 | 75.92 |
| Total | 100.21 | 99.97 | 99.89 | Ga | 12.29 | 10.35 | 24.39 |
| K ₂ O+Na ₂ O | 7.86 | 7.49 | 7.72 | Rb | 130.66 | 200.65 | 294.88 |
| A/NK | 1.27 | 1.51 | 1.46 | Sr | 116.65 | 102.45 | 118.67 |
| A/CNK | 1.01 | 1.21 | 1.17 | Zr | 43.29 | 200.66 | 304.54 |
| La | 25.63 | 52.30 | 65.79 | Nb | 3.05 | 10.67 | 21.44 |
| Ce | 38.92 | 89.68 | 131.31 | Mo | 0.08 | 0.12 | 0.74 |
| Pr | 4.14 | 8.77 | 15.37 | Cd | 0.09 | 0.14 | 0.16 |
| Nd | 17.33 | 32.10 | 59.91 | In | 0.05 | 0.08 | 0.10 |
| Sm | 2.87 | 8.67 | 11.52 | Cs | 2.12 | 8.67 | 9.96 |
| Eu | 0.52 | 0.92 | 1.08 | Ba | 632.13 | 710.23 | 618.77 |
| Gd | 4.19 | 8.64 | 10.09 | Hf | 1.67 | 8.60 | 10.21 |
| Tb | 0.81 | 1.24 | 1.63 | Ta | 0.87 | 1.69 | 2.35 |
| Dy | 4.76 | 6.86 | 9.04 | W | 363.73 | 320.00 | 1.75 |
| Ho | 1.11 | 2.31 | 1.58 | Tl | — | — | 1.92 |
| Er | 2.55 | 4.95 | 4.55 | Pb | 34.50 | 42.73 | 56.72 |
| Tm | 0.38 | 0.68 | 0.82 | Bi | 0.08 | 0.06 | 1.32 |
| Yb | 2.56 | 4.46 | 4.37 | Th | 16.63 | 35.60 | 48.94 |
| Lu | 0.42 | 0.46 | 0.68 | U | 3.64 | 5.44 | 6.67 |

图解上显示 Rb、Th、U 和 K 正异常以及 Ba、Nb、Ta、Sr、P 和 Ti 负异常(图 7b), 与壳源岩浆岩的地球化学特征一致(Rudnick et al., 2003)。尖山子似斑状花岗岩 $\varepsilon_{\text{Hf}}(t)$ 值为 $-5.19 \sim -1.59$, 与已报道的同时期花岗质岩石相似(叶晓峰等, 2013; Liu et al., 2015; Yuan et al., 2015; Soldner et al., 2019; Wang et al., 2021b), 这些新元古代早期花岗质岩石共同显示演化的 Hf 同位素组成, 且这些岩石结晶锆石以及捕获或残留锆石 $\varepsilon_{\text{Hf}}(t)$ 值主要落在 2.2~1.3 Ga 地壳物质 Hf 同位素演化区内(图 5)。上述全岩主量微量元素和锆石 Hf 同位素特征反应北山造山带南部新元古代早期花岗质岩石主

要起源于地壳, 指示了早期地壳的再造事件。这与同时期一些过铝质花岗岩属于 S-型花岗岩相一致, 这些 S-型花岗岩常常含有过铝质矿物, 如白云母、石榴子石(姜洪颖等, 2013; Wang et al., 2021b)。此外, Zong 等(2017)在古堡泉和旧井地区报道了 ~ 900 Ma 角闪岩相变质事件, 这也与北山南部新元古代早期地壳再造事件相一致。

5.2 北山造山带南部前寒武纪基底的构造亲缘性

北山造山带经历了古生代构造、变质和岩浆事件的强烈叠加和改造, 能够标志微陆块性质的前寒武纪基底大多呈碎片分布于古生代的岩浆弧地体中(图 1b;

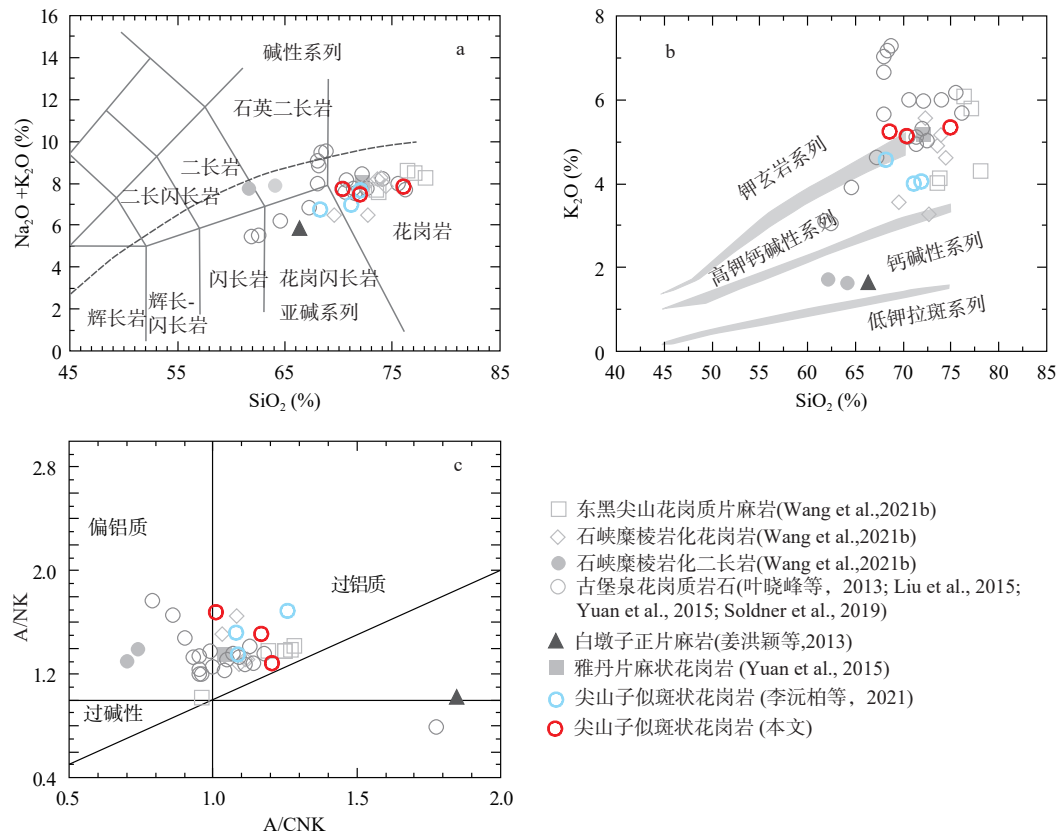
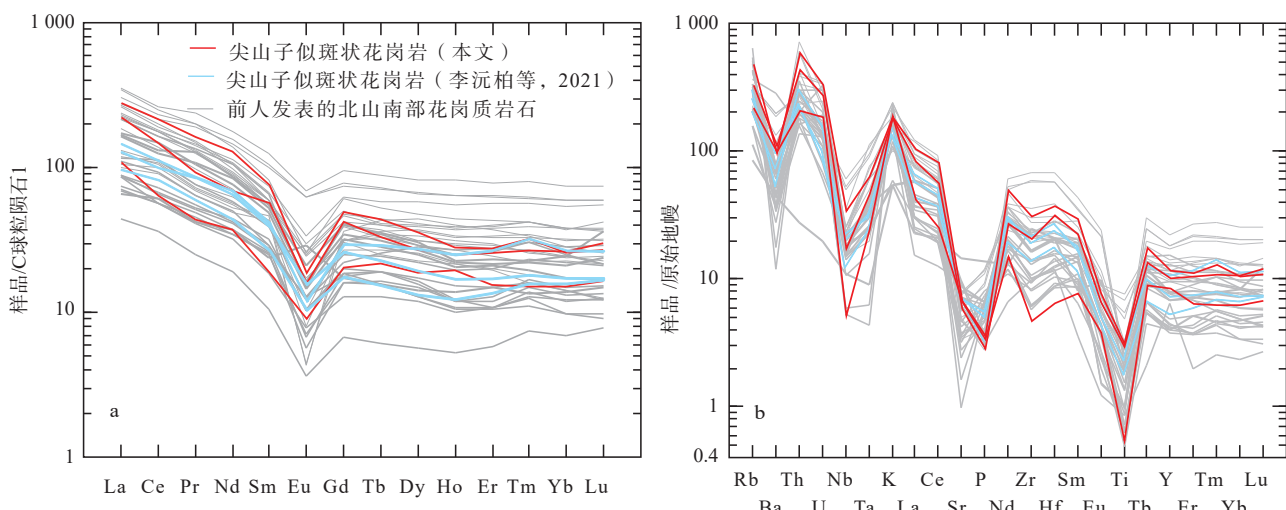


图6 尖山子似斑状花岗岩(a)硅-碱性图(据 Middlemost, 1994), (b)SiO₂-K₂O图(据 Frost et al., 2001)和(c)A/NK-A/CNK图(据 Maniar et al., 1989)

Fig. 6 (a) Total alkali versus silica diagram, (b) SiO_2 vs K_2O plot and (c) A/NK vs A/CNK diagram of the porphyritic granite in the Jianshanzi area.



北山造山带南部已发表的新元古代花岗质岩石微量元素数据来自叶晓峰等(2013); 姜洪颖等(2013); Liu 等(2015); Yuan 等(2015); Soldner 等(2019); Wang 等(2021b); C₁球粒陨石和原始地幔值据 Sun 等(1989)

图7 尖山子似斑状花岗岩C_i球粒陨石标准化稀土元素配分图(a)和原始地幔标准化多元素图(b)

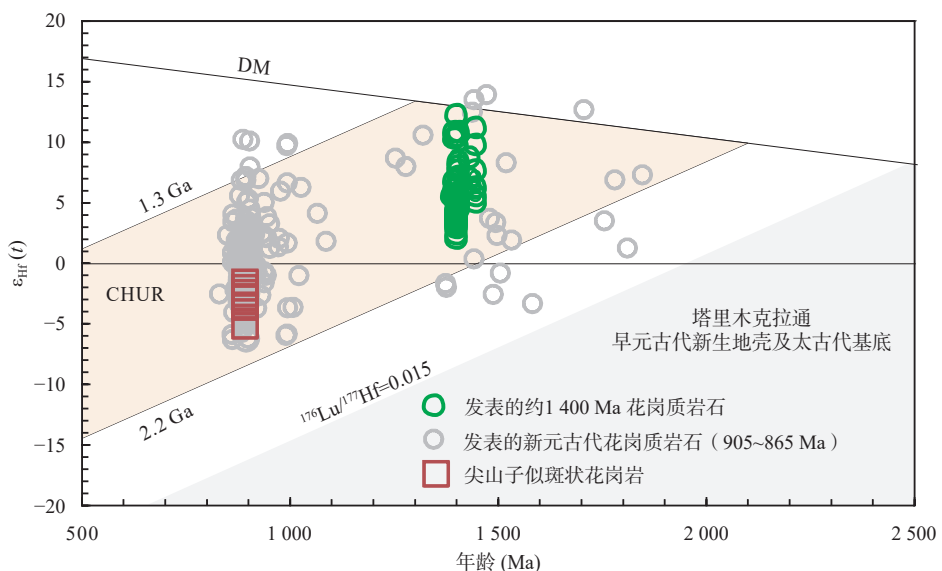
C₁ chondrite-normalized REE patterns and (b) primitive mantle-normalized incompatible trace element variations.

of the porphyritic granite in the Jianshanzi area

Xiao et al., 2010; He et al., 2018)。长期以来,将分布在北山不同构造单元上的中高级变质岩即“北山杂岩”看作前寒武纪基底,并依据岩石地层对比和少量的全岩 Sm-Nd 等时线年龄、Ar-Ar 年龄和单颗粒锆石 U-Pb 上交点年龄(主要获得 2.9~1.6 Ga),认为北山造山带南部前寒武纪基底具有塔里木克拉通或敦煌微陆块的亲缘性(左国朝等,1990; Zuo et al., 1991; 何世平等,2005; 杨合群等,2008,2009,2010,2012)。

然而,近年来识别出具有确切年龄的前寒武纪岩石为新元古代岩浆岩和~1400 Ma 花岗质片麻岩

(图 1b)。~1400 Ma 花岗质片麻岩显示了地壳的新生事件(图 8; 贺振宇等,2015; He et al., 2018; Yuan et al., 2019),而出露的多处新元古代花岗质岩石显示了地壳的再造事件(叶晓峰等,2013; 姜洪颖等,2013; Liu et al., 2015; Yuan et al., 2015; Wang et al., 2021b)。然而,这些岩石锆石 $\epsilon_{\text{Hf}}(t)$ 值主体落在 2.2~1.3 Ga 地壳物质 Hf 同位素演化区内(图 8),暗示北山造山带南部前寒武纪基底可能不存在太古代的基底。因此,它们可能不具有塔里木克拉通的构造亲缘性,因为塔里木克拉通广泛发育太古代的结晶基底(朱文斌等,2022)。



图中数据来自姜洪颖等(2013); 叶晓峰等(2013); 贺振宇等(2015); Liu 等(2015); Yuan 等(2015); Wang 等(2021b); Yuan 等(2019)及本文

图8 北山造山带南部中元古代和新元古代早期花岗质岩石锆石 $\epsilon_{\text{Hf}}(t)$ -年龄(Ma)图解

Fig. 8 The zircon $\epsilon_{\text{Hf}}(t)$ versus age (Ma) plot for the Mesoproterozoic and Neoproterozoic granitic rocks in the southern Beishan Orogenic Belt

6 结论

(1) 北山造山带南部广泛发育新元古代早期岩浆事件。尖山子似斑状花岗岩锆石 U-Pb 年龄分别为 (901 ± 5) Ma 和 (935 ± 3) Ma。尖山子似斑状花岗岩地球化学特征与北山南部花岗质岩石地球化学特征相似, 反应了新元古代早期地壳再造事件。

(2) 北山造山带南部经历了中元古代地壳新生和新元古代早期地壳再造事件, 锆石 $\epsilon_{\text{Hf}}(t)$ 值主要落在 2.2~1.3 Ga 地壳物质 Hf 同位素演化区内, 可能暗示不存在太古代的基底, 即前寒武纪基底与具有太古代结晶基底的塔里木克拉通可能不同。

致谢: 感谢审稿专家提出的宝贵修改意见, 在此致以诚挚的感谢。李树才、曹军、杨兵、黄福勇等参加了部分野外工作, 在此一并致以谢意。

参考文献(References):

- 卜涛, 王国强, 黄博涛, 等. 北山北带新元古代 A 型花岗岩: Rodinia 超大陆裂解早期的地质响应 [J]. 岩石学报, 2022, 38(10): 2988~3002.
 BU Tao, WANG Guoqian, HUANG Botao, et al. Neoproterozoic A-type granites in northern Beishan Orogenic Belt: Early response of the Rodinia supercontinent break-up [J]. Acta Petrologica Sinica, 2022, 38(10): 2988~3002.
- 戴鹏飞, 苟学明, 何大鹏, 等. 北山南部炭窑井地区花岗岩型铀

- 矿地质特征及找矿模型[J]. 东华理工大学学报(自然科学版), 2023, 46(1): 10–20.
- DAI Pengfei, GOU Xueming, HE Dapeng, et al. Geological characteristics and prospecting model of granite-type uranium deposits in Tanyaojing area, southern Beishan[J]. Journal of East China University of Technology (Natural Science), 2023, 46(1): 10–20.
- 贺振宇, 孙立新, 毛玲娟, 等. 北山造山带南部片麻岩和花岗闪长岩的锆石 U-Pb 定年和 Hf 同位素: 中元古代的岩浆作用与地壳生长[J]. 科学通报, 2015, 60(4): 389–399.
- HE Zhenyu, SUN Lixin, MAO Lingjuan, et al. Zircon U-Pb and Hf isotopic study of gneiss and granodiorite from the southern Beishan orogenic collage: Mesoproterozoic magmatism and crustal growth[J]. Chinese Science Bulletin, 2015, 60(4): 389–399.
- 何世平, 任秉琛, 姚文光, 等. 甘肃内蒙古北山地区构造单元划分[J]. 西北地质, 2002, 35(4): 30–40.
- HE Shiping, REN Bingchen, YAO Wenguang, et al. The division of tectonic units of Beishan area, Gansu-Inner Mongolia[J]. Northwestern Geology, 2002, 35(4): 30–40.
- 何世平, 周会武, 任秉琛, 等. 甘肃内蒙古北山地区古生代地壳演化[J]. 西北地质, 2015, 38(3): 6–15.
- HE Shiping, ZHOU Huiwu, REN Bingchen, et al. Crustal evolution of Paleozoic in Beishan area, Gansu and Inner Mongolia, China[J]. Northwestern Geology, 2015, 38(3): 6–15.
- 霍宁, 郭谦谦, 陈艺超, 等. 北山中部古硐井群物源区性质与构造意义[J]. 岩石学报, 2022, 38(4): 1253–1279.
- HUO Ning, GUO Qianqian, CHEN Yichao et al. Provenance and tectonic setting of the Gudongjing Group in Beishan Orogen[J]. Acta Petrologica Sinica, 2022, 38(4): 1253–1279.
- 姜洪颖, 贺振宇, 宗克清, 等. 北山造山带南缘北山杂岩的锆石 U-Pb 定年和 Hf 同位素研究[J]. 岩石学报, 2013, 29(11): 3949–3967.
- JIANG Hongying, HE Zhenyu, ZONG Keqing, et al. Zircon U-Pb dating and Hf isotopic studies on the Beishan complex in the southern Beishan Orogenic Belt[J]. Acta Petrologica Sinica, 2013, 29(11): 3949–3967.
- 李怀坤, 朱士兴, 相振群, 等. 北京延庆高于庄组凝灰岩的锆石 U-Pb 定年研究及其对华北北部中元古界划分新方案的进一步约束[J]. 岩石学报, 2010, 26(7): 2131–2140.
- LI Huikun, ZHU Shixing, XIANG Zhenqun, et al. Zircon U-Pb dating on tuff bed from Gaoyuzhuang Formation in Yanqing, Beijing: Further constraints on the new subdivision of the Mesoproterozoic stratigraphy in the northern North China Craton[J]. Acta Petrologica Sinica, 2010, 26(7): 2131–2140.
- 李志琛. 敦煌地块变质岩系时代新认识[J]. 中国区域地质, 1994, 13(2): 131–134.
- LI Zhichen. New speculation of the age of the metamorphic rocks series of the Dunhuang massif[J]. Regional Geology of China, 1994, 13(2): 131–134.
- 李沅柏, 李海泉, 周文孝, 等. 北山造山带新元古代热事件及其构造意义: 来自甘肃北山南带两期花岗质岩的地球化学和年代学证据[J]. 地质通报, 2021, 40(7): 1117–1139.
- LI Yuanbai, LI Haiquan, ZHOU Wenxiao, et al. Neoproterozoic thermal events and tectonic implications in the Beishan orogenic belt: Geochemical and geochronological evidence from two sets of granitic rocks from the southern Beishan orogenic belt, Gansu Province[J]. Geological Bulletin of China, 2021, 40(7): 1117–1139.
- 梅华林, 于海峰, 李铨, 等. 甘肃敦煌-北山早前寒武纪岩石组合构造初步框架[J]. 前寒武纪研究进展, 1997, 20(4): 47–54.
- MEI Hualin, YU Haifeng, LI Quan. Preliminary litho-tectonic framework of early Precambrian rocks in Dunhuang-Beishan area, Gansu, west China[J]. Progress in Precambrian Research, 1997, 20(4): 47–54.
- 梅华林, 李惠民, 陆松年, 等. 甘肃柳园地区花岗质岩石时代及成因[J]. 岩石矿物学杂志, 1999, 18(1): 14–17.
- MEI Hualin, LI Huimin, LU Songnian, et al. The age and origin of the Liuyuan granitoid, northwestern Gansu[J]. Acta Petrologica et Mineralogica, 1999, 18(1): 14–17.
- 聂凤军, 江思宏, 刘妍, 等. 内蒙古北山交叉沟地区变质火山岩 Sm-Nd 同位素研究[J]. 地质学报, 2004, 76(8): 807–812.
- NIE Fengjun, JIANG Sihong, LIU Yan, et al. Sm-Nd isotope study on metamorphosed volcano-sedimentary Rocks of the Jiaochagou Metamorphic Complex, Beishan Mt., Inner Mongolia[J]. Acta Geologica Sinica, 2004, 76(8): 807–812.
- 牛文超, 任邦方, 任云伟, 等. 北山北带新元古代岩浆记录: 来自内蒙古哈珠地区片麻状花岗岩的证据[J]. 地球科学, 2019, 44(1): 284–297.
- NIU Wenchao, REN Bangfang, REN Yunwei, et al. Neoproterozoic magmatic records in the north Beishan Orogenic Belt: evidence of the gneissic granites from the Hazhu area, Inner Mongolia[J]. Earth Science, 2019, 44(1): 284–297.
- 牛腾, 倪志耀, 孟宝航, 等. 冀北康保芦家营巨斑状花岗岩: 华北克拉通北缘中段 1.3~1.2 Ga B. P. 伸展—裂解事件的地质记录[J]. 成都理工大学学报(自然科学版), 2023, 50(4): 486–503.
- NIU Teng, NI Zhiyao, MENG Baohang, et al. The Lujiaying megaporphyrlic granite in Kangbao area, North Hebei: A geological record of extension and breakup event at 1.3~1.2 Ga B. P. in the central segment of northern margin of North China Craton [J]. Journal of Chengdu University of Technology (Science & Technology Edition), 2023, 50(4): 486–503.
- 桑海清, 裴冀, 王松山, 等. 北山地区大口子片麻岩 Ar-Ar 年代学初步研究[J]. 地球学报, 1997, 18(S1): 58–61.
- SANG Haiqing, QIU Ji, WANG Songshan, et al. A preliminary study on Ar-Ar chronology of Dakouzi gneiss from Beishan Area[J]. Acta Geoscientia Sinica, 1997, 18(S1): 58–61.
- 孙新春, 张红军, 魏志军, 等. 甘蒙北山地区小红山一带变质侵入岩体的时代厘定及其地质意义[J]. 西北地质, 2005, 38(3): 61–67.
- SUN Xinchun, ZHANG Hongjun, WEI Zhijun, et al. Time of defini-

- tion and geological meaning for metamorphic intrusive rock body in Xiaohongshan region, Beishan area of Gansu and Inner Mongolia[J]. *Northwestern Geology*, 2005, 38(3): 61–67.
- 魏学平, 龚全胜, 梁明宏, 等. 马鬃山隆起区前长城系敦煌岩群变质变形和演化特征[J]. 甘肃地质学报, 2000, 9(1): 36–43.
- WEI Xueping, GONG Quansheng, LIANG Minghong, et al. Metamorphic deformational and evolutionary characteristics of pre-Changcheng Dunhuang terrain occurring on Mazongshan up-welling area[J]. *Acta Geologica Gansu*, 2000, 9(1): 36–43.
- 王文宝, 李卫星, 雷聪聪, 等. 中亚造山带中段早—中三叠世埃达克岩和A型花岗岩成因及构造意义[J]. 西北地质, 2024, 57(3): 29–43.
- WANG Wenbao, LI Weixing, LEI Congcong, et al. Early-Middle Triassic Adakitic and A-type Granite in Middle Segment of Central Asian Orogenic Belt: Petrogenesis and Tectonic Implications[J]. *Northwestern Geology*, 2024, 57(3): 29–43.
- 王梓桐, 王根厚, 张维杰, 等. 阿拉善地块南缘志留纪花岗闪长岩LA-ICP-MS锆石U-Pb年龄及地球化学特征[J]. 成都理工大学学报(自然科学版), 2022, 49(5): 586–600.
- WANG Zitong, WANG Genhou, ZHANG Weijie, et al. LA-ICP-MS zircon U-Pb dating and geochemical characteristics of the Silurian granodiorite in the southern margin of Alxa Block, China[J]. *Journal of Chengdu University of Technology (Science Technology Edition)*, 2022, 49(5): 586–600.
- 吴妍蓉, 周海, 赵国春, 等. 中亚造山带南蒙古地区石炭纪—二叠纪岩浆活动及其构造意义[J]. 西北地质, 2024, 57(3): 11–28.
- WU Yanrong, ZHOU Hai, ZHAO Guochun, et al. Carboniferous-Permian Magmatism of Southern Mongolia, Central Asian Orogenic Belt and Its Tectonic Implications[J]. *Northwestern Geology*, 2024, 57(3): 11–28.
- 肖文交, 宋东方, Windley B F, 等. 中亚增生造山过程与成矿作用研究进展[J]. 中国科学: 地球科学, 2019, 49(10): 1512–1545.
- XIAO Wenjiao, SONG Dongfang, Windley B F, et al. Research progresses of the accretionary processes and metallogenesis of the Central Asian Orogenic Belt[J]. *Science China: Earth Sciences*, 2019, 49(10): 1512–1545.
- 杨合群, 李英, 李文明, 等. 北山成矿构造背景概论[J]. *西北地质*, 2008, 41(1): 22–28.
- YANG Hequn, LI Ying, LI Wenming, et al. General discussion on metallogenic tectonic setting of Beishan Mountain, Northwestern China[J]. *Northwestern Geology*, 2008, 41(1): 22–28.
- 杨合群, 李英, 赵国斌, 等. 新疆-甘肃-内蒙古衔接区地层对比及其意义[J]. *西北地质*, 2009, 42(4): 60–75.
- YANG Hequn, LI Ying, ZHAO Guobin, et al. Stratigraphic Correlation and Its Significance of Xinjiang-Gansu-Inner Mongolia Join Area[J]. *Northwestern Geology*, 2009, 42(4): 60–75.
- 杨合群, 李英, 赵国斌, 等. 北山蛇绿岩特征及构造属性[J]. 西北地质, 2010, 43(1): 26–35.
- YANG Hequn, LI Ying, ZHAO Guobin, et al. Character and structural attribute of the Beishan ophiolite[J]. *Northwestern Geology*, 2010, 43(1): 26–35.
- 杨合群, 赵国斌, 李英, 等. 新疆-甘肃-内蒙古衔接区古生代构造背景与成矿的关系[J]. 地质通报, 2012, 31(2/3): 413–421.
- YANG Hequn, ZHAO Guobin, LI Ying, et al. The relationship between Paleozoic tectonic setting and mineralization in Xinjiang-Gansu-Inner Mongolia juncture area[J]. *Geological Bulletin of China*, 2012, 31(2/3): 413–421.
- 叶晓峰, 宗克清, 张泽明, 等. 北山造山带南缘柳园地区新元古代花岗岩的地球化学特征及其地质意义[J]. 地质通报, 2013, 32(2–3): 307–317.
- YE Xiaofeng, ZONG Keqing, ZHANG Zeming, et al. Geochemistry of Neoproterozoic granite in Liuyuan area of southern Beishan orogenic belt and its geological significance[J]. *Geological Bulletin of China*, 2013, 32(2–3): 307–317.
- 俞胜, 赵斌斌, 贾轩, 等. 北山造山带南缘一条山北闪长岩地球化学、年代学特征及其构造意义[J]. 西北地质, 2022, 55(4): 267–279.
- YU Sheng, ZHAO Binbin, JIA Xuan, et al. Geochemistry, Geochronology Characteristics and Tectonic Significance of Yitiaoshan Diorite in the Southern Margin of Beishan Orogenic Belt[J]. *Northwestern Geology*, 2022, 55(4): 267–279.
- 朱文斌, 林和丰, 葛荣峰, 等. 塔里木克拉通北缘库鲁克塔格地块太古宙基底组成与地壳演化[J]. 地质学报, 2022, 96(9): 3084–3101.
- ZHU Wenbin, LIN Hefeng, GE Rongfeng, et al. Archean basement composition and crustal evolution of the Kuluketage block in the northern margin of the Tarim Craton[J]. *Acta Geologica Sinica*, 2022, 96(9): 3084–3101.
- 左国朝, 张淑玲, 何国琦, 等. 北山地区早古生代板块构造特征[J]. 地质科学, 1990, 4: 305–314.
- ZUO Guochao, ZHANG Shuling, HE Guoqi, et al. Early Paleozoic plate tectonics in Beishan area[J]. *Chinese Journal of Geology*, 1990, 4: 305–314.
- Ao S J, Xiao W J, Windley B F, et al. Paleozoic accretionary orogenesis in the eastern Beishan orogen: constraints from zircon U-Pb and $^{40}\text{Ar}/^{39}\text{Ar}$ geochronology[J]. *Gondwana Research*, 2016, 30: 224–235.
- Frost B R, Barnes C G, Collins W J, et al. A geochemical classification for granitic rocks[J]. *Journal of Petrology*, 2001, 42(11): 2033–2048.
- He Z Y, Klemd R, Yan L L, et al. The origin and crustal evolution of microcontinents in the Beishan orogen of the southern Central Asian Orogenic Belt[J]. *Earth-Science Reviews*, 2018, 185: 1–14.
- Huang B T, Wang G Q, Li X M, et al. Precambrian tectonic affinity of the Beishan Orogenic Belt: Constraints from Proterozoic metasedimentary rocks[J]. *Precambrian Research*, 2022, 376: P106686.
- Kröner A, Alexeiev D V, Agramonte Y, et al. Mesoproterozoic

- (Grenvilleage) terranes in the Kyrgyz North Tianshan: zircon ages and Nd-Hf isotopic constraints on the origin and evolution of basement blocks in the southern Central Asian Orogen[J]. *Gondwana Research*, 2013, 23: 272–295.
- Li J, Wu C, Chen X, et al. Tectonic setting of metamorphism and exhumation of eclogite-facies rocks in the South Beishan orogen, northwestern China[J]. *Geosphere*, 2023, 19(1): 100–138.
- Liu Q, Zhao G C, Sun M, et al. Ages and tectonic implications of Neoproterozoic ortho- and paragneisses in the Beishan Orogenic Belt, China[J]. *Precambrian Research*, 2015, 266: 551–578.
- Maniar P D, Piccoli P M. Tectonic discrimination of granitoids[J]. *Geological Society of America Bulletin*, 1989, 101: 635–643.
- Middlemost E A. Naming materials in the magma/igneous rock system[J]. *Earth Science Reviews*, 1994, 37(3–4): 215–224.
- Niu Y Z, Shi G R, Ji W H, et al. Paleogeographic evolution of a Carboniferous-Permian sea in the southernmost part of the Central Asian Orogenic Belt, NW China: Evidence from microfacies, provenance and paleobiogeography[J]. *Earth-Science Reviews*, 2021a, 220: 103738.
- Niu Y Z, Shi G R, Wang J Q, et al. The closing of the southern branch of the Paleo-Asian Ocean: Constraints from sedimentary records in the southern Beishan region of the Central Asian Orogenic Belt, NW China[J]. *Marine and Petroleum Geology*, 2021b, 124: 104791.
- Rudnick R L, Gao S. Composition of the continental crust. In: Rudick R L. The crust, treatise on geochemistry, Amsterdam[M]. Elsevier, 2003, 3: 1–64.
- Sengör A M C, Natal'in B A, Burtman V S. Evolution of the Altaiid tectonic collage and Palaeozoic crustal growth in Eurasia[J]. *Nature*, 1993, 364: 299–307.
- Song D F, Xiao W J, Han C M, et al. Progressive accretionary tectonics of the Beishan orogenic collage Altaiids: insights from zircon U-Pb and Hf isotopic data of high-grade complexes[J]. *Precambrian Research*, 2013a, 227: 368–388.
- Song D F, Xiao W J, Han C M, et al. Geochronological and geochemical study of gneiss-schist complexes and associated granitoids, Beishan Orogen, southern Altaiids[J]. *International Geology Review*, 2013b, 55(14): 1705–1727.
- Song D F, Xiao W J, Han C M, et al. Provenance of meta-sedimentary rocks from the Beishan orogenic collage, southern Altaiids: constraints from detrital zircon U-Pb and Hf isotopic data[J]. *Gondwana Research*, 2013c, 24: 1127–1151.
- Song D F, Xiao W J, Windley B F, et al. A Paleozoic Japan-type subduction-accretion system in the Beishan orogenic collage, southern Central Asian Orogenic Belt[J]. *Lithos*, 2015, 224–225: 195–213.
- Song D F, Xiao W J, Windley B F, et al. Metamorphic complexes in accretionary orogens: insights from the Beishan collage, southern Central Asian Orogenic Belt[J]. *Tectonophysics*, 2016, 688: 135–147.
- Soldner J, Yuan C, Schulmann K, et al. Grenvillian evolution of the Beishan Orogen, NW China: Implications for development of an active Rodinian Margin[J]. *The Geological Society of American*, 2019, 132(7–8): 1657–1680.
- Sun S S, McDonough W F. Chemical and isotopic systematics of oceanic basalts: implications for mantle composition and processes[M]. In: Saunders, A. D., Norry, M. J. (Eds.), *Magmatism in the Ocean Basins*. Geological Society, London, Special Publications, 1989, 42, 313–345.
- Windley B F, Alexeiev D, Xiao W J, et al. Tectonic models for accretion of the Central Asian Orogenic Belt[J]. *Journal of the Geological Society*, 2007, 164: 31–47.
- Xiao W J, Mao Q G, Windley B F, et al. Paleozoic multiple accretionary and collisional processes of the Beishan orogenic collage[J]. *American Journal of Science*, 2010, 310: 1553–1594.
- Yuan Y, Zong K Q, He Z Y, et al. Geochemical and geochronological evidence for a former early Neoproterozoic microcontinent in the South Beishan Orogenic Belt, southernmost Central Asian Orogenic Belt[J]. *Precambrian Research*, 2015, 266: 409–424.
- Yuan Y, Zong K Q, Cawood P A, et al. Implication of Mesoproterozoic (~1.4 Ga) Magmatism within microcontinents along the southern Central Asian Orogenic Belt[J]. *Precambrian Research*, 2019, 327: 314–326.
- Zheng R G, Li J Y, Xiao W J, et al. Nature and provenance of the Beishan Complex, southernmost Central Asian Orogenic Belt [J]. *International Journal of Earth Sciences*, 2018, 107: 729–755.
- Zhou J B, Wilde S A, Zhao G C, et al. Nature and assembly of microcontinental blocks within the Paleo-Asian Ocean[J]. *Earth-Science Reviews*, 2018, 186: 76–93.
- Zong K Q, Klem R, Yuan Y, et al. The assembly of Rodinia: The correlation of early Neoproterozoic (ca. 900 Ma) high-grade metamorphism and continental arc for Mation in the southern Beishan Orogen, southern Central Asian Orogenic Belt (CAOB) [J]. *Precambrian Research*, 2017, 290: 32–48.
- Zuo G C, Zhang S L, He G Q, et al. Plate tectonic characteristics during the early Paleozoic in Beishan near the Sino-Mongolian border region, China[J]. *Tectonophysics*, 1991, 188: 385–392.
- Wang B R, Yang X S, Li S C, et al. Age, depositional environment, and tectonic significance of an Early Neoproterozoic volcano-sedimentary sequence in the eastern Beishan orogenic belt, southern Central Asian Orogenic Belt[J]. *Geological Journal*, 2021a, 156: 1346–1357.
- Wang B R, Yang X S, Li S C, et al. Geochronology, geochemistry, and tectonic implications of early Neoproterozoic granitic rocks from the eastern Beishan Orogenic Belt, southern Central Asian Orogenic Belt[J]. *Precambrian Research*, 2021b, 352: 106016.